

HEALTH AND MEDICINE

A unique biomimetic modification endows polyetherketoneketone scaffold with osteoinductivity by activating cAMP/PKA signaling pathway

Bo Yuan^{1,2}, Yuxiang Zhang^{1,2}, Rui Zhao^{1,2}, Hai Lin^{1,2}, Xiao Yang^{1,2}, Xiangdong Zhu^{1,2*}, Kai Zhang^{1,2,3*}, Antonios G. Mikos⁴, Xingdong Zhang^{1,2,3}

Osteoinductivity of a biomaterial scaffold can notably enhance the bone healing performance. In this study, we developed a biomimetic and hierarchically porous polyetherketoneketone (PEKK) scaffold with unique osteoinductivity using a combined surface treatment strategy of a sulfonated process and a nano bone-like apatite deposition. In a beagle intramuscular model, the scaffold induced bone formation ectopically after 12-week implantation. The better bone healing ability of the scaffold than the original PEKK was also confirmed in orthotopic sites. After culturing with bone marrow-derived mesenchymal stem cells (BMSCs), the scaffold induced osteogenic differentiation of BMSCs, and the new bone formation could be mainly depending on cell signaling through adenylyl cyclase 9, which activates the cyclic adenosine monophosphate/protein kinase A signaling cascade pathways. The current work reports a new osteoinductive synthetic polymeric scaffold with its detailed molecular mechanism of action for bone repair and regeneration.

INTRODUCTION

Repair of load-bearing large bone defects caused by trauma and disease still presents clinical challenge (1–3). Transplantation of autografts has long been recognized to be the gold standard and the most effective method for bone repair and regeneration, but it has drawbacks such as limited bone supply and donor site morbidity (4, 5). Allografts lack these complications but have the risk of disease transfer and immunogenicity (4). A promising therapeutic approach is the application of bone tissue engineering, in which growth factors and in vitro expanded cells are incorporated into biomaterial scaffolds to achieve the biological functions by inducing tissue regeneration (6, 7). However, bone tissue engineering requires high-cost and extensive ex vivo cell manipulation and has difficulties in clinical translation and regulatory approval. A promising, effective, and practical strategy is to develop a new generation of tissue-inducing biomaterial that can eliminate the need for growth factors and exogenous cells and induce in situ bone tissue regeneration (8–10).

The definition of tissue-inducing biomaterial, “a biomaterial designed to induce the regeneration of damaged or missing tissues or organs without the addition of cells and/or bioactive factors” (11), stems from the osteoinduction of biomaterials that was found by Winter and Simpson (12) in 1969 in a subcutaneous implantation of polyhydroxyethyl methacrylate (poly-HEMA) sponge. However, the landmark finding and its significance for tissue regeneration have not yet been given sufficient scientific attention because the synthetic biomaterial as a biologically inert substance at that time only simply repaired the physical shape of bone defects. With the rapid development of biomedical science and improved understanding of regenerative medicine, the role of synthetic biomaterial

used for bone grafts has shifted from a biologically passive and structural role to one in which materials could orchestrate the biological process of bone regeneration (13–16). In the early 1990s, our group and Ripamonti successively reported the initial histological evidence of the osteoinduction calcium phosphate (CaP) ceramics in a variety of animal species (17–19), initiating a new age in osteoinductive biomaterials for bone regeneration.

In addition to osteoinductivity, biomaterials for load-bearing bone repair require mechanical properties to maintain stability and facilitate bone tissue regeneration. Although porous CaP ceramics demonstrated a similar performance with that of both autologous bone and growth factors in repairing critical-sized bone defects and spinal fusion (20, 21), the inherent brittleness still limits their application in load-bearing sites. Some surface-modified porous metals also induce bone regeneration (22–24), while the porous metals had the relatively weak osteoinduction ability and potential issues of stress shielding and radiopaque in clinical practice. Compared with ceramic and metal materials, polymeric materials have more versatile physicochemical properties to suit their clinical applications and are thus gradually replacing metallic materials as the leading implant materials for medical applications such as spinal fusion and craniofacial procedures (7, 25). However, to the best of our knowledge, except poly-HEMA sponge (12), no other polymer has been found to induce bone regeneration without the addition of bioactive factors and/or cells.

Polyaryletherketones (PAEKs), a class of high-performance thermoplastic polymers, have been widely used in the fields of orthopedics and spine due to its excellent mechanical properties, chemical resistance, and natural radiolucency (25). However, the poor osteointegration of PAEKs due to their inert nature hampers the long-term stability and clinical outcomes of PAEK implants (26). To overcome their bioinert issue, we modified the polyetherketoneketone (PEKK; a representative PAEK material) surface by constructing a bone-like apatite coating to endow its high bioactivity and in vivo osteointegration ability (27). In addition, we prepared a biomimetic PEKK scaffold by mimicking the hierarchical microporous structure of the natural bone in another study (28). Our in vitro and

Copyright © 2022
The Authors, some
rights reserved;
exclusive licensee
American Association
for the Advancement
of Science. No claim to
original U.S. Government
Works. Distributed
under a Creative
Commons Attribution
NonCommercial
License 4.0 (CC BY-NC).

¹National Engineering Research Center for Biomaterials, Sichuan University, Chengdu 610064, P. R. China. ²School of Biomedical Engineering, Sichuan University, Chengdu 610064, P. R. China. ³Institute of Regulatory Science for Medical Device, Sichuan University, Chengdu 610064, P. R. China. ⁴Departments of Bioengineering and Chemical and Biomolecular Engineering, Rice University, Houston, TX 77251, USA. *Corresponding author. Email: zhu_xd1973@scu.edu.cn (X. Zhu); kaizhang@scu.edu.cn (K.Z.)

in vivo results confirmed that the biomimetic PEKK scaffold had a hierarchically porous architecture and mechanical strength similar to that of osteoporotic trabecular bone and could thus rapidly match with host bone and facilitate osteoporotic bone regeneration.

In this study, inspired by the tissue-inducing biomaterial and hierarchically porous architecture of natural trabecular bone, we developed a biomimetic PEKK scaffold for load-bearing bone repair by using a wet chemical modification and biomimetic mineralization method (Fig. 1A). In a beagle intramuscular implantation model, we found that the biomimetic PEKK scaffold could induce bone formation ectopically after 12 weeks of implantation. In vitro cell culture using bone marrow-derived mesenchymal stem cells (BMSCs) showed that adenylyl cyclase 9 (ADCY9)/cyclic adenosine monophosphate (cAMP)/protein kinase A (PKA) signaling cascade played a crucial role in the biomimetic PEKK scaffold-induced bone regeneration.

RESULTS

Preparation and characterization of biomimetic porous PEKK scaffolds

Biomimetic porous PEKK scaffolds with bone-like apatite coating (PEKK-B) was prepared in two steps, as illustrated in Fig. 1B. Sulfonation

treatment was used to introduce a microporous network and hydrophilic $-SO_3H^-$ groups on the pore walls of PEKK, which provided multiple nucleation sites for the in situ self-assembly of bone-like apatite in simulated body fluid (SBF). We first characterized the architecture of the as-prepared scaffolds via microcomputed tomography (μ -CT). Both the PEKK and PEKK-B scaffolds had a similar interconnected porous structure and porosity to natural trabecular bone (Fig. 1C and fig. S1A). The surface of the unmodified PEKK was smooth and dense, whereas similar hierarchical microporous network such as natural trabecular bone was created on the surface of the PEKK-B scaffold by sulfonated treatment (Fig. 1D and fig. S1B).

Moreover, high-magnification scanning electron microscopy (SEM) images revealed that this microporous network was covered by uniformly dispersed bone-like apatite clusters, which is similar to the bone collagen matrix network embedded beneath osteoblast-secreted nanohydroxyapatite. The cross-sectional SEM images of the PEKK-B scaffold showed that the thickness of the apatite coating consisting of nanosheets (~ 15 nm) was approximately $4 \mu\text{m}$ (fig. S1, C and D). The surface nanopopography of the scaffolds was further visualized by atomic force microscopy (AFM). As shown in Fig. 1 (E and F), the PEKK-B scaffold had similar nanoscale texturing

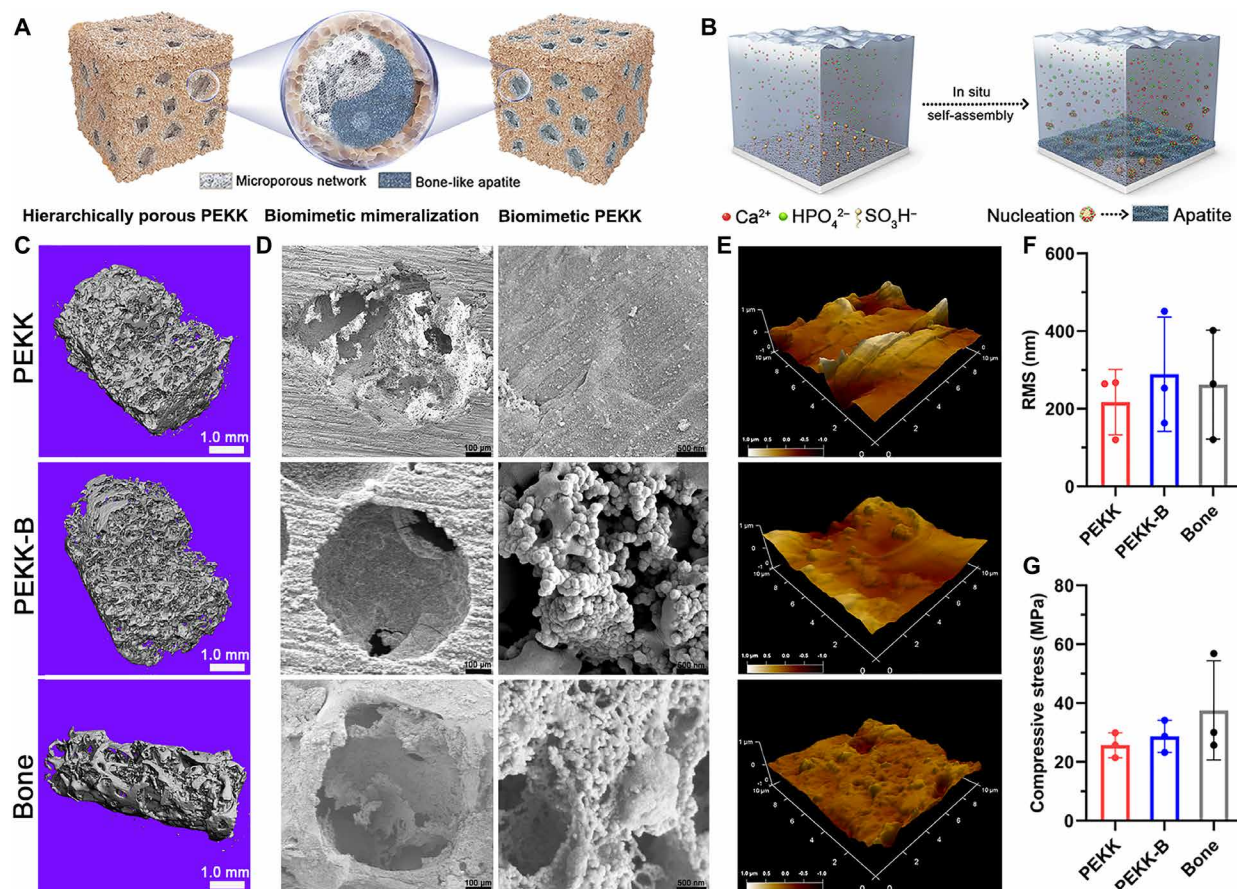


Fig. 1. Preparation and characterization of the biomimetic PEKK-B materials. (A) Schematic illustration of the preparation of biomimetic PEKK scaffold. (B) In situ self-assembly of bone-like apatite nanoparticles on the microporous network of sulfonated PEKK scaffold. (C) Microcomputed tomography (μ -CT) reconstruction and (D) scanning electron microscopy (SEM) observation for various PEKK scaffolds and natural trabecular bone. (E) Typical atomic force microscopy (AFM) images and (F) corresponding surface roughness of PEKK scaffolds and natural trabecular bone. (G) Compressive strength of PEKK scaffolds and natural trabecular bone (error bars, means \pm SD; $n = 3$ per group). All analyses were done using one-way analysis of variance (ANOVA) with Tukey's post hoc test.

and roughness to those of the natural bone matrix. In addition, the similar macroporous structure between the PEKK scaffolds and trabecular bone resulted in similar compressive strength (Fig. 1G).

PEKK-B induces bone regeneration at heterotopic and orthotopic sites

To evaluate the osteoinductive ability of the PEKK scaffolds, cylindrically shaped scaffolds (size, $\Phi 5 \times 8 \text{ mm}^3$) were implanted into the dorsal muscle of the beagle. Figure 2A shows the timeline and arrangement of the *in vivo* experiments. We first visualized ectopic bone formation within the scaffolds during 24 weeks of implantation by μ -CT. As shown in Fig. 2B, during the whole implantation period, a newly formed bone was detected only in the PEKK-B group, while no sign of bone formation was found in the PEKK group. To verify the μ -CT results, we further analyzed histological staining for the implants retrieved at 12 and 24 weeks postoperatively (Fig. 2C and fig. S2). At 24 weeks after implantation, fibrous connective tissues had grown into the pores of the PEKK scaffold without any new bone formation. However, for PEKK-B, a small amount of bone tissue was found in the inner pores and closely attached to the pore walls at 12 weeks after implantation (fig. S2). With the prolongation of the implantation period, much more new bone formed in the inner pores of the PEKK-B scaffold, accompanied by many mature osteocytes embedded inside bone lacunae. SEM and energy-dispersive spectrometry analysis further confirmed that the induced new bone had directly bonded to the scaffold surface, which contained both calcium and phosphorus. We further calculated the incidence of bone formation induced by PEKK-B. At 12 and 24 weeks, ectopic bone formation was observed in the PEKK-B group in 5 of 10 and 9 of 10, respectively (Fig. 2D). In addition, according to the quantitative analysis of new bone tissue, the newly formed bone in the inner pores of the PEKK-B scaffolds increased gradually with implantation time (Fig. 2, E and F).

In addition to ectopic bone formation, the bone regeneration ability of the biomimetic porous PEKK-B scaffold at intraosseous locations was also investigated. After implantation in beagle femoral defects for 12 weeks, a large amount of new bone formed within the defects of the PEKK-B scaffold, leading to a complete bridging between the scaffold and the adjacent bones (Fig. 2, G and H). According to the quantitative analysis for new bone, at 12 weeks, the bone ingrowth area and the bone ingrowth volume of the PEKK-B scaffold were 3.05- and 4.07-fold significantly higher than those of the PEKK, respectively.

PEKK-B promotes the osteogenic differentiation of BMSCs via ADCY9/cAMP/PAK signaling

The effect of material properties on tissue regeneration is mediated via cell-material interactions, and therefore, we decided to analyze the effect of the PEKK scaffolds on osteogenic differentiation of BMSCs *in vitro*. We first observed the morphology of BMSCs cultured on the scaffolds by SEM after 1 day of culture. As shown in Fig. 3A, BMSCs cultured on PEKK presented an extended shape that was attached to the smooth surface by elongated filopodia. However, BMSCs grown on the PEKK-B scaffold showed a flattened polygonal morphology with outstretched lamellipodia anchored to the nanosheets. Accordingly, a larger cell area was measured in the PEKK-B scaffold than that in the PEKK scaffold (Fig. 3B). Furthermore, confocal laser scanning microscopy (CLSM) observation revealed that a great number of live cells with few dead cells adhered

to the surface and further migrated into the pores of the scaffolds (fig. S3). Although both PEKK and PEKK-B groups showed an increased cell density with culture time, more cells and more-spread cell morphology were observed in the PEKK-B group throughout the culture period (Fig. 3C and fig. S4A). As determined by the Cell Counting Kit-8 (CCK-8) assay, cell proliferation occurred for all scaffolds across the period examined, while the cell viability of BMSCs in the PEKK-B group was significantly higher than that in PEKK group at days 3 and 5 (Fig. 3D). Furthermore, we investigated the effects on key osteogenic gene expression in BMSCs cultured with the scaffolds via quantitative reverse transcription polymerase chain reaction (qRT-PCR). After 5 days of culture, cells in the PEKK-B group demonstrated strongly up-regulated genes, including alkaline phosphatase (ALP), collagen I (COL I), osteocalcin (OCN), runt-related transcription factor 2 (Runx-2), and bone sialoprotein (BSP). The degree of extracellular matrix mineralization on different PEKK scaffolds was examined using Alizarin Red S staining (fig. S4B). The PEKK-B group showed a significantly higher mineralization degree than the PEKK and control groups, suggesting stronger osteogenic differentiation potential.

To investigate the molecular mechanism for BMSCs osteogenic differentiation induced by the PEKK-B scaffold, we performed an in-depth mRNA expression profile microarray on day 3 of culture. Principal components analysis was used to reduce all assessment variables into three principal components that accounted for most of the variability within the data, allowing for two-dimensional visualization of the entire dataset (29). Scatterplots of the first three principal components demonstrated clear separation of control group from material groups (PEKK-B and PEKK) along the principal component 1 and 2 (PC1 and PC2) axis (Fig. 4A). Further *t*-distributed stochastic neighbor embedding cluster analysis of all three samples revealed three distinct clusters (30), suggesting a clear difference in gene expression among the three samples (Fig. 4B). Compared to the control group, more than 9900 genes were extensively regulated in the material groups, including 4637 up-regulated genes and 5302 down-regulated genes ($P < 0.05$; 1.5 fold changes as the cutoff) (fig. S5). Of the regulated genes, 2278 genes up-regulated and 4246 genes down-regulated overlapped in the two material groups. Further comparison suggested that more than 600 genes were significantly regulated in the PEKK-B group compared to the PEKK group, including 333 up-regulated genes and 338 down-regulated genes (the abbreviations and full names of some genes are provided in table S1) (Fig. 4C). Among them, PEKK-B significantly up-regulated the expression of genes involved in biological regulation and signal transduction {ADCY9, CXCR1 [chemokine (C-X-C motif) receptor1], PGF (placental growth factor), and ADRB1 (adrenergic receptor, beta 1)} and genes belonging to positive regulation of cell differentiation [MAP2K2 (mitogen-activated protein kinase kinase 2), PRKACA (protein kinase catalytic alpha), Runx-2, and interleukin-17A (IL-17A)]. In addition, genes involved in cellular calcium transport [ADRB3, GNA11 (guanine nucleotide binding protein, alpha 11), GNAS (guanine nucleotide binding protein, alpha stimulating), PKT2B (protein tyrosine kinase 2 beta), SLC8A1 [solute carrier family 8 (sodium/calcium exchanger), member 1], and CAMK2A (calcium/calmodulin-dependent protein kinase II alpha)] were also expressed differentially.

To identify the pathways involved, we carried out gene set enrichment analysis using multiple databases including the Gene Ontology (GO) database and the Kyoto Encyclopedia of Genes and Genomes database. There were a total nine up-regulation-related pathways in

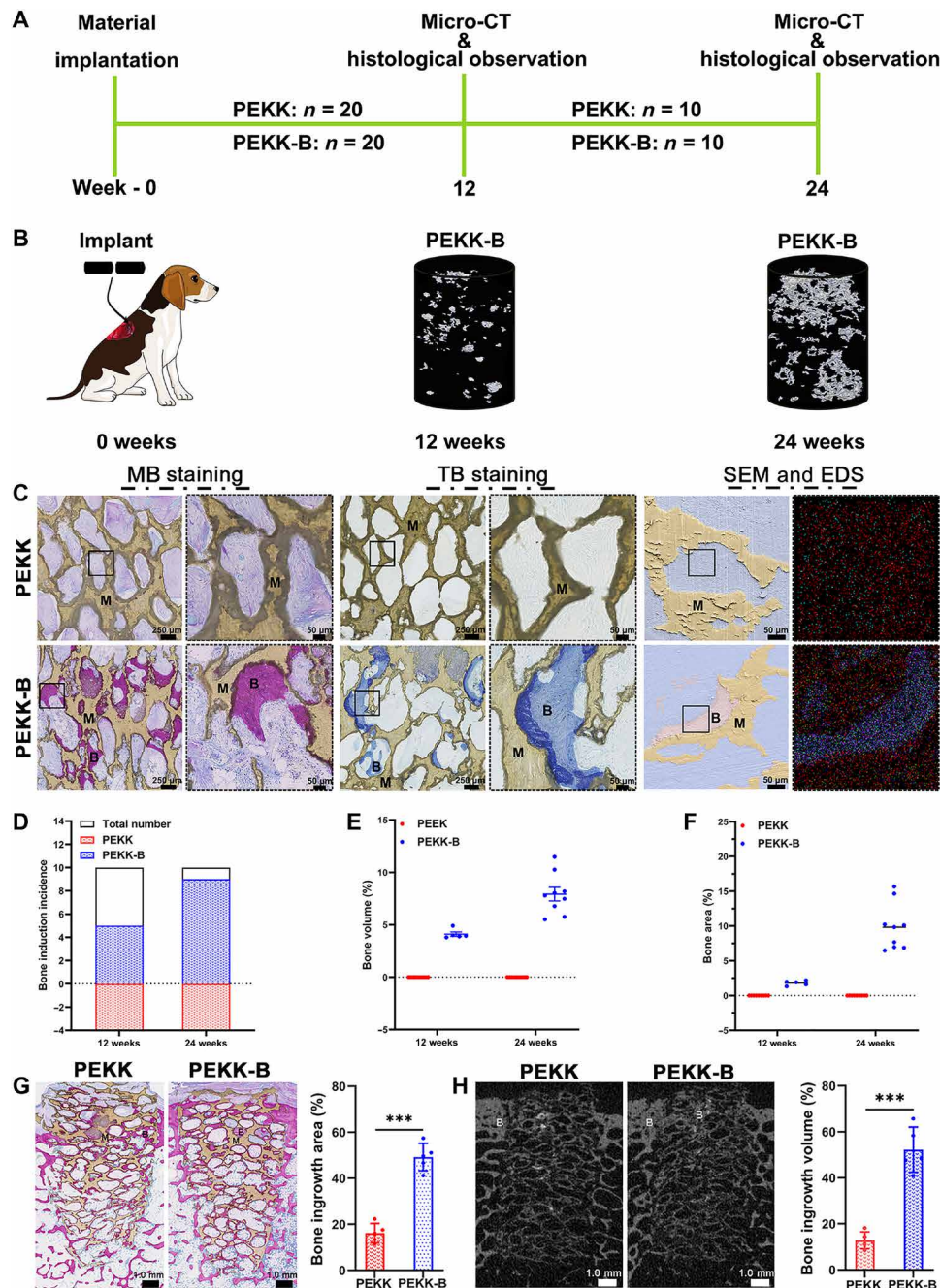


Fig. 2. Evaluation of the bone formation in heterotopic and orthotopic sites induced by the PEKK scaffold. (A) Timeline and arrangement of the in vivo experiments. (B) Implantation site of the scaffold and the μ -CT evaluation of new bone (white) formation within the scaffold. (C) Histological analysis for new bone formation within the scaffold (M, material; B, bone tissue). EDS, energy-dispersive spectrometry. (D) Bone induction incidence of the scaffold. (E) Quantitative analysis of the volume and (F) area fraction of new bone formation within the scaffold. (G) Hematoxylin and eosin staining of histological sections and quantitative analysis of the volume fraction of new bone formation within different PEKK scaffolds at week 12 postoperatively (M, material; B, bone tissue). (H) μ -CT evaluation and quantitative analysis of the volume fraction of new bone formation (gray) within different PEKK scaffolds at week 12 postoperatively (error bars, means \pm SD; $n = 10$ per group; all analyses were done using unpaired Student's *t* test). *** $P < 0.001$.

the PEKK-B group versus the PEKK group, which could be divided into three components: (i) positive regulation of cell proliferation and differentiation: phospholipase D, phosphoinositide 3-kinase (Pi3K)-AKT, cyclic guanosine monophosphate-dependent protein kinase (cGMP-PKG), and Janus kinase-signal transducer and activator of transcription (JAK-STAT) signaling pathways; (ii) calcium homeostasis: calcium signaling, endocrine and other factor-regulated calcium

reabsorption, and cAMP signaling pathways (Fig. 4, D and E); and (iii) other signaling pathways. Unexpectedly, ADCY9, an adenylate cyclase, was involved in multiple signaling pathways including cAMP, phospholipase D, cGMP-PKG, and endocrine and other factor-regulated calcium reabsorption signaling pathways, appearing to be a central mediator of material-mediated BMSC osteogenic differentiation. We further verified the expression of some key genes involved in

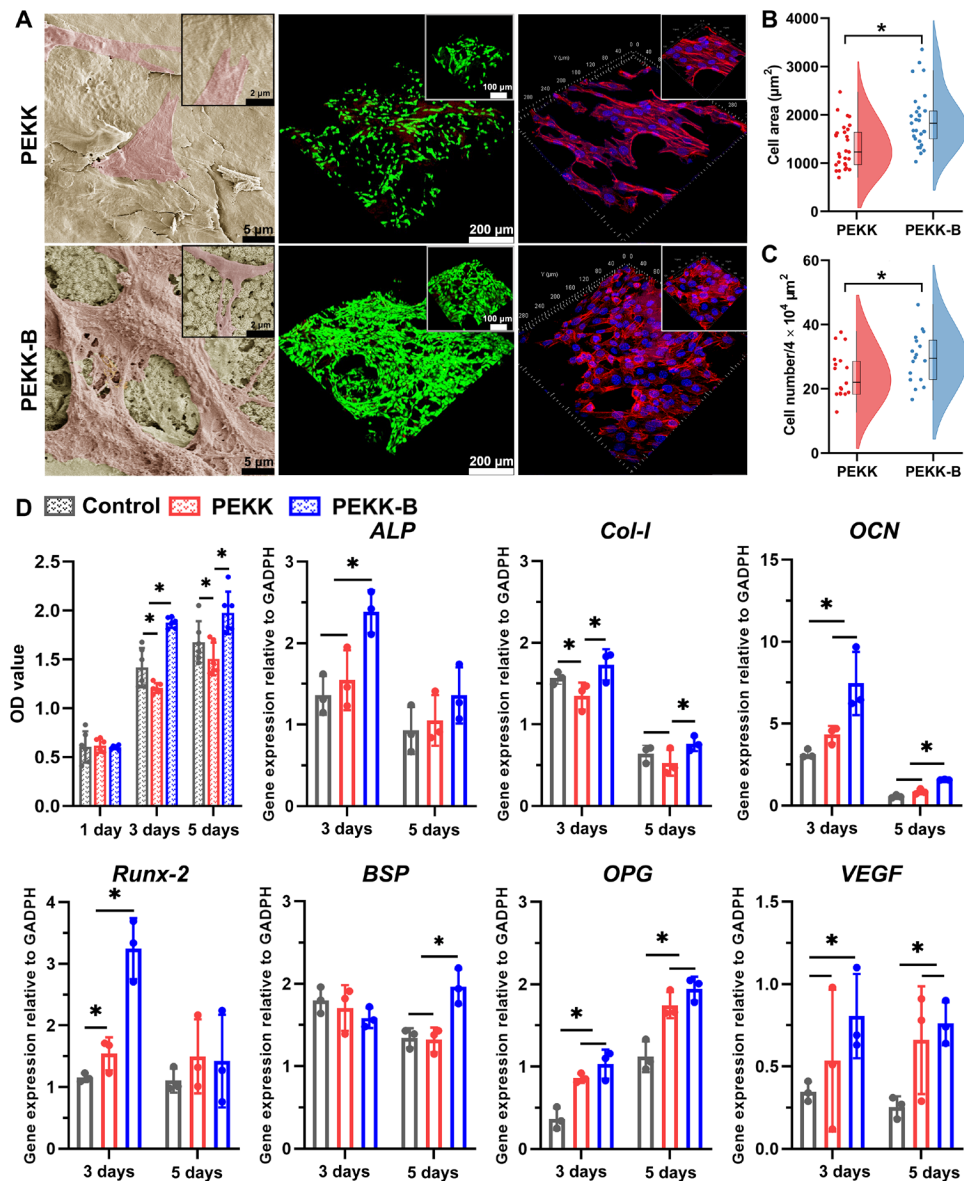


Fig. 3. Effect of the scaffolds on osteogenic differentiation of BMSCs in vitro. (A) SEM and CLSM observations and (B) the corresponding quantitative assay of the cell area and (C) cell number of BMSCs cultured on the scaffolds for 1 day (actin filament is stained red, while the cell nuclei are stained blue). (D) Cell viability of BMSCs cultured on the scaffolds at days 1, 3, and 5, and several osteogenic gene expressions of BMSCs cultured on the scaffolds at days 3 and 5 (error bars, means \pm SD; $n = 6$ per group for cell viability test; $n = 3$ per group for qRT-PCR analysis). All analyses were done using one-way ANOVA with Tukey's post hoc test. * $P < 0.05$ and *** $P < 0.001$.

these signaling pathways by performing qRT-PCR and found that the expression levels of six genes (CXCR1, PGF, ADCY9, MAP2K1, PRKACA, and SLC20 α 1) in the PEKK-B were much higher than that in the control and PEKK groups (Fig. 4F). Among them, ADCY9 and PRKACA were the key mediators of the cAMP/PKA signaling pathway, suggesting that PEKK-B might regulate osteogenic differentiation of BMSCs via the ADCY9/cAMP/PKA signaling.

To validate this hypothesis, we first analyzed whether PEKK-B was able to activate cAMP signaling in BMSCs and its potential downstream targets by Western blotting. As shown in Fig. 5 and fig. S6, compared with control and PEKK, PEKK-B significantly promoted the expression of the key mediators in cAMP signaling including ADCY9, cAMP, and PKA and increased the phosphorylation

level of downstream mitogen-activated protein kinase kinase (MEK), extracellular signal-regulated kinase (ERK), and cAMP response element-binding protein (CREB). The protein expression of ALP, an early osteogenesis marker, of BMSCs in PEKK-B was much higher than that in the control and PEKK group. Then, we further treated BMSCs with *N*-(2-(*p*-bromocinnamylamino)ethyl)-5-isoquinoline-sulfonamide-2HCl hydrate (H89; an inhibitor of PKA activity) or 9-(tetrahydrofuran-2-yl)-9*H*-purin-6-amine (SQ22536; an inhibitor of ADCY activity) and evaluated their effects on material-mediated osteogenic differentiation. In the presence of H89 or SQ22536, the PEKK-B-mediated up-regulation of phosphorylation levels of MEK, ERK, and CREB was significantly reduced. Furthermore, the expression of ALP protein of BMSCs treated with H89 or SQ22536

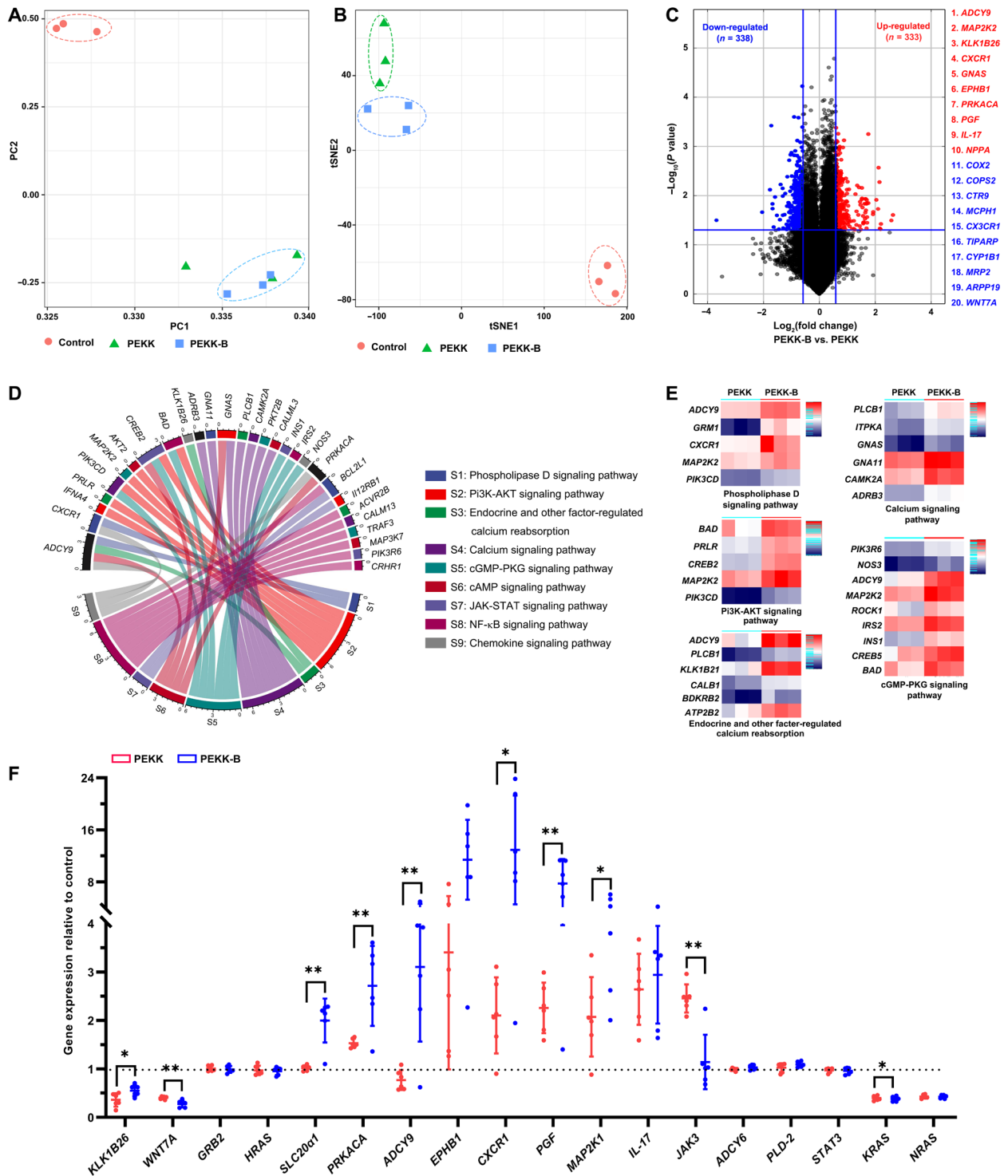


Fig. 4. Analysis of cell signaling pathways mediated by the scaffolds during the osteogenic differentiation of BMSCs. (A) Principal components analysis and (B) *t*-distributed stochastic neighbor embedding (tSNE) cluster analysis of BMSCs cultured on the scaffolds at day 3. (C) Volcano plot showing differentially regulated genes in the PEKK-B as compared to the PEKK group. Genes with an absolute fold change of >1.5 and a *P* value of <0.05 are highlighted in green and red, denoting down- and up-regulated genes, respectively. (D) Circular visualization of the results of gene-annotation enrichment analysis. (E) Heatmap of genes that were differentially expressed in PEKK-B versus PEKK group with a fold change of >1.5 and a *P* value of <0.05. (F) qRT-PCR validation for representative genes (error bars, means ± SD; *n* = 6 per group; all analyses were done using unpaired Student’s *t* test). **P* < 0.05 and ***P* < 0.01.

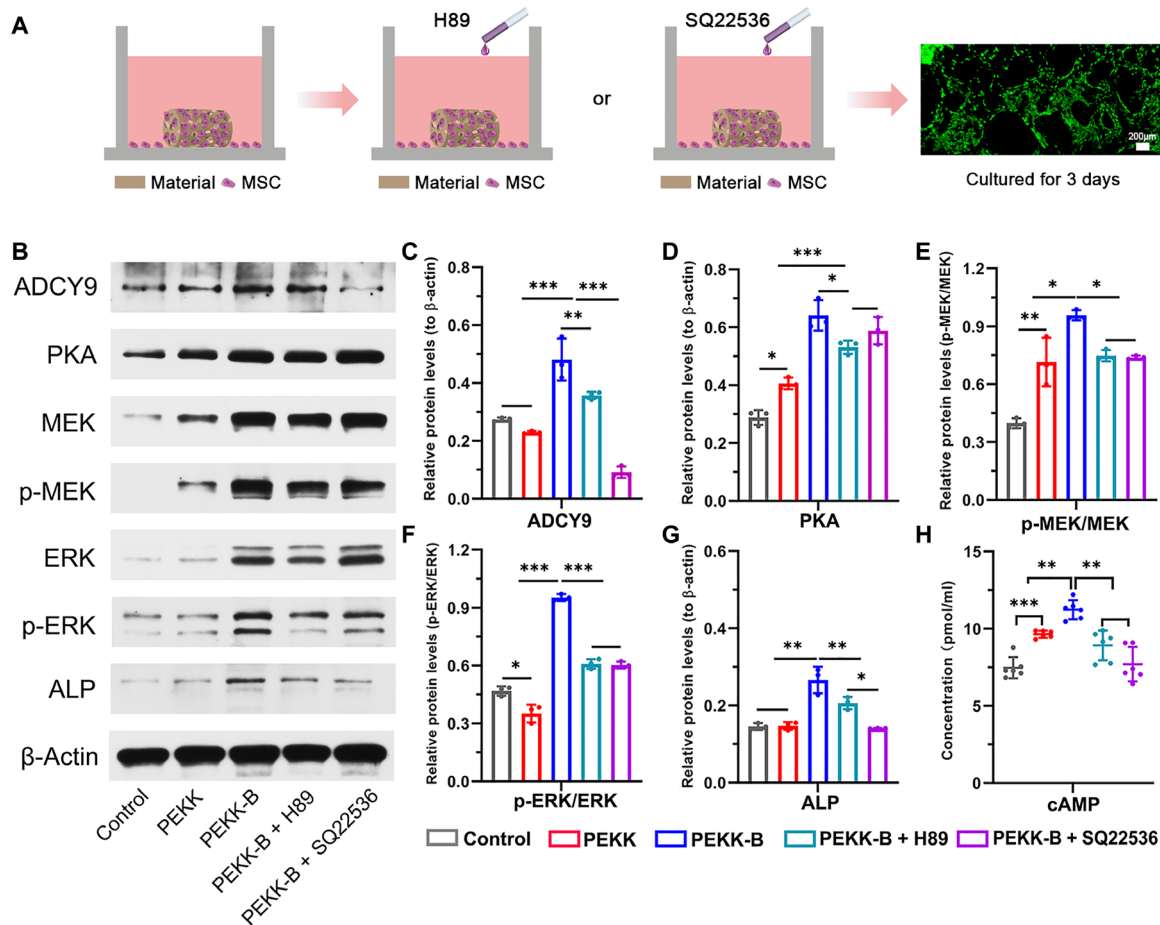


Fig. 5. Regulation of ADCY9/cAMP/PKA signaling activated by the scaffolds on BMSCs osteogenic differentiation. (A) Schematic of the scaffolds cultured with BMSCs treated by PAK inhibitor H89 or ADCY inhibitor SQ22536 for 3 days. (B) Western blot analysis of ADCY9, PKA, MEK/p-MEK, ERK/p-ERK, ALP, and β-actin and (C to G) the corresponding quantitative analysis of band intensities. (H) Relative expression of cAMP in BMSCs as assessed by enzyme-linked immunosorbent assay kit (error bars, means \pm SD; $n = 3$ per group; all analyses were done using one-way ANOVA with Tukey's post hoc test). * $P < 0.05$, ** $P < 0.01$, and *** $P < 0.001$.

was significantly inhibited. Note that PEKK-B showed decreased relative intracellular concentration of the upstream cAMP when the downstream PKA was inhibited, which might be attributed to the feedback regulation of PKA on cAMP (31, 32). Therefore, the above results suggested that PEKK-B induced osteogenic differentiation of BMSCs primarily by ADCY9/cAMP/PKA signaling pathway and phosphorylation of downstream MEK/ERK/CREB signaling.

PEKK-B induces bone formation in heterotopic site by cAMP/PKA-activated BMSCs

To evaluate the effect of cAMP/PKA signaling activated by the scaffold on in vivo bone formation, the PEKK scaffolds loaded with BMSCs treated with different inhibitors were cultured for 3 days and implanted into the leg muscle of the mouse (Fig. 6A). After 90 days, three of the five PEKK-B scaffolds were filled with a large amount of new bone tissue, where many mature osteocytes embedded in the matrix structure (Fig. 6B). In contrast, no sign of bone formation was found within the PEKK-B scaffold in the presence of PKA inhibitor H89 or ADCY inhibitor SQ22536. In addition, although many blood vessels were homogeneously distributed in the pores of the PEKK scaffold, there was no new bone tissue formation. Consistent with

this finding, we found that the expression level of OCN, an osteogenic marker, was significantly higher in PEKK-B scaffold than in PEKK scaffold, while treatment with H89 or SQ22536 significantly reduced OCN activity in PEKK-B scaffold (Fig. 6C). These results suggested that the PEKK-B scaffold could activate the cAMP/PKA signaling of BMSCs to induce bone formation in heterotopic site.

DISCUSSION

Osteoinductive materials offer great potential for the repair and regeneration of load-bearing bone defects (33). However, the clinical application of now available osteoinductive ceramics and metals has been limited by their flexibility in regulating both mechanical properties and osteoinductive ability. Compared with ceramics and metals, polymers offer more possibilities for chemical modifications and structure alterations that could facilitate tailoring of the material properties to meet the clinical requirements (7, 34, 35). However, in the past five decades since Winter and Simpson (12) first reported ectopic bone formation induced by poly-HEMA sponge in 1969, developing osteoinductive polymers remains a huge challenge as demonstrated by the lack of experimental and mechanistic studies and reports.

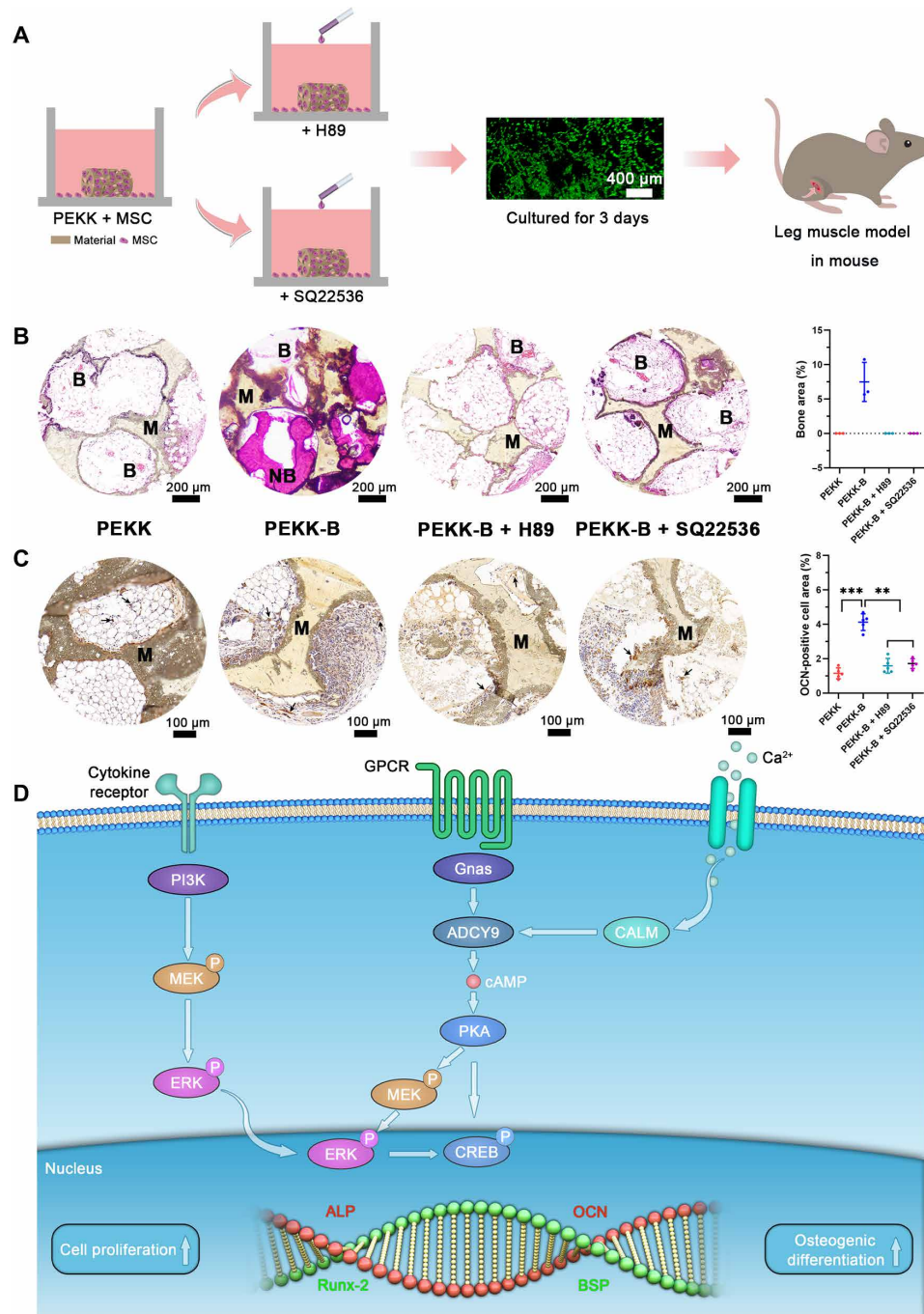


Fig. 6. The scaffolds induce bone formation ectopically by cAMP/PKA-activated BMSCs. (A) Schematic illustration of the implanted scaffolds loaded with BMSCs treated with different inhibitors. (B) Histological analysis for new bone formation within the scaffold at day 90 postoperatively (M, material; B, blood vessel; NB, newly formed bone). (C) Immunohistochemical staining for the osteogenic marker OCN (brown, black arrow). (D) Schematic diagram of the molecular mechanism for BMSCs osteogenic differentiation induced by the PEKK-B scaffold (error bars, means \pm SD; $n = 5$ per group; all analyses were done using one-way ANOVA with Tukey's post hoc test). ** $P < 0.01$ and *** $P < 0.001$.

The observations made over the past decades in the field of osteoinductive ceramics and metals have revealed that three-dimensionally interconnected macropores, abundant surface micropores, and rapid bone-like apatite formation under physiological condition were the requisite material factors for materials-induced bone formation (36, 37). Inspired by these observations accumulated

from multiple studies and reports on osteoinductive ceramics and metals, we prepared a biomimetic PEKK-B scaffold with a hierarchically porous architecture and mechanical strength similar to that of natural trabecular bone using a sulfonated treatment followed by a biomimetic mineralization process (Fig. 1). The highly plastic structure in the PEKK scaffold enables its mechanical properties to

be regulated by optimizing the size, distribution, and amount of the pores depending on target defect sites. According to the previous reports, the regulation range of the tensile strength of the PEKK scaffold was approximately 28 to 71 MPa, which could meet the mechanical requirements for repairing load-bearing bone defects (38, 39). The finding that significant ectopic bone formation was found within the PEKK-B scaffold after implantation in the dorsal muscle of beagle for 12 weeks suggested that altering both the physical structure and surface chemistry of bioinert PEKK could endow it with excellent osteoinductivity (Fig. 2). The hierarchically porous architecture and high osteoinductive activity promoted the PEKK-B scaffold rapid integration with host bone and induced bone tissue ingrowth and thus achieved healing of load-bearing bones (fig. S3).

Although osteoinductive materials represented by CaP ceramics have been successfully commercialized and achieved good clinical outcomes in non-load-bearing bone defects, the mechanism underlying osteoinduction by synthetic biomaterials is not yet fully understood. The induced bone formation by PEKK-B could be ascribed to the synergistic stimulating effect of the hierarchically porous architecture and surface bone-like apatite. On one hand, the hierarchically porous structure could increase the scaffold's specific surface area and thus promote the adsorption of osteogenesis-related proteins, which was favorable for the recruitment and osteoblastic differentiation of BMSCs. On the other hand, the released Ca^{2+} and PO_4^{3-} ions from the surface apatite layer could also promote the differentiation of BMSCs (36, 37, 40). Although many studies by our and other groups have confirmed that osteoinductive materials could stimulate the expression of bone morphogenetic protein 2 (BMP-2) or other signaling molecules in MSCs to promote its osteogenic differentiation (41–43), how osteoinductive materials stimulate MSCs to secrete these signaling molecules is still largely unknown. As reported by Siddappa *et al.* (44), the activation of cAMP/PKA signaling in BMSCs could elicit an immediate response through induction of genes such as ID2 and FosB to sustained secretion of bone-related cytokines such as BMP-2 and IL-11, resulting in ectopic bone formation. In line with this report, we also found that PEKK-B could promote BMSCs differentiation by activating the cAMP/PKA and downstream MEK/ERK/CREB signaling to induce the ectopic bone formation, suggesting that cAMP/PKA signaling cascade might be one of the pivotal pathways in regulating the secretion of osteogenic-related cytokines in BMSCs.

Our findings indicated that ADCY9 played a key role in the osteogenic differentiation of BMSCs driven by activated cAMP/PKA signaling cascade. Among the nine transmembrane isoforms of adenylate cyclase, ADCY6 has been shown to be required for load-induced bone formation *in vivo*, while ADCY9 is typically considered associated with immune response (45, 46). However, ADCY6 did not appear to have a positive effect in PEKK-B-induced BMSCs osteogenic differentiation (Fig. 4). Considering the Ca^{2+} -mediated potentiation of ADCY9 (47), it is reasonable to speculate that the released Ca^{2+} ions from PEKK-B scaffold may enter cells through calcium channels and calcium-sensing receptors and activated the ADCY9/cAMP/PKA signaling cascade and other cytokines to modulate the osteogenic differentiation of BMSCs (Fig. 6D). In addition to Ca^{2+} ions, PO_4^{3-} groups have also been shown to be capable of entering the cells via solute carrier family 20 member 1 (SLC20a1) and promote the osteogenic differentiation of BMSCs by regulating intramitochondrial phosphate content and adenosine triphosphate synthesis (48). Similarly, our study also found that the

expression level of SLC20a1 was significantly up-regulated in PEKK-B, indicating the potential role of PO_4^{3-} groups in activating cAMP/PKA signaling cascade.

In summary, this study successfully developed osteoinductive PEKK scaffolds and further elucidated that the mechanism of osteoinduction is related to the activation of ADCY9/cAMP/PKA signaling cascade. Along with our previous systematic research on osteoinductive ceramics and metals (24, 36), new findings of this report on osteoinductive polymers made further progresses to piece the osteoinductive puzzle of synthetic biomaterials by confirming that introducing hierarchically biomimetic macroporous architecture with abundant surface micropores and bone-like apatite coating could alter biological properties of PEEK scaffolds from bioinertness to osteoinductivity. The biomimetic PEKK scaffold is a promising candidate for load-bearing bone defects repair and spinal fusion. Furthermore, our current work provides new insights into the mechanisms of action for osteoinduction using synthetic polymers, which will be beneficial for developing a new generation of osteoinductive polymeric biomaterials and devices.

MATERIALS AND METHODS

Sample preparation

The preparation of porous PEKK was performed according to the following procedure. Briefly, PEKK powder (Arylmax K7500, Polymics, USA) and HA (hydroxyapatite) microspheres (Engineering Research Center in Biomaterials, Sichuan University, China) in a 5:1 mass ratio were thoroughly mixed with an appropriate amount of ethanol to form a slurry. The as-prepared slurry was transferred to a custom-built mold and then compressed at 55 MPa and 362°C for 30 min to achieve a composite. After immersing in 37% HCl solution for 4 hours, the HA microspheres within the composite were leached, and thus, the PEKK scaffold with equivalent pore size and porosity was obtained. Then, the porous PEKK sample was immersed in 85% sulfuric acid solution for 30 min and ultrasonically cleaned in deionized water for 15 min to obtain the sulfonated porous PEKK. A bone-like apatite coating was synthesized *in situ* on the microporous of sulfonated PEKK scaffolds by the chemical precipitation method in an SBF. The SBF was prepared as described in our previous study (38) and filtered-sterilized using a 0.2- μm filter. The as-obtained sulfonated PEKK scaffolds were transferred to a sterile centrifuge tube that contained SBF and then placed in an incubator at 37°C for 5 days. A layer of bone-like apatite coating on the microporous network of sulfonated PEKK was obtained after washing in deionized water for several times. In this study, the PEKK scaffolds with dimensions of $\Phi 14 \times 2 \text{ mm}^3$ and $\Phi 5 \times 8 \text{ mm}^3$ were prepared for material characterization and *in vitro* (or *in vivo*) study, respectively.

Material characterization

The porous structure of the PEKK scaffolds was visualized by a $\mu\text{-CT}$ system (SCANCO vivaCT 80, Switzerland). A field-emission SEM (FE-SEM; S4800, Hitachi, Japan) was used to observe the morphologies of the scaffolds. The surface nanotopography and roughness of the scaffolds were further investigated by an AFM (Asylum Research, MFP-3D, USA) operating in tapping mode at ambient conditions with a resonant frequency of 75 kHz. The test values for the RMS (root-mean-square) were calculated by averaging the values obtained from four nonoverlapping sample regions (10 μm

by 10 μm). The pore size distribution and porosity of the scaffolds were evaluated by a mercury intrusion porosimetry (AutoPore IV9500, Micromeritics, USA). Three parallel samples of each group were used in the above tests.

Surgical procedure

The animal experiments in the present study were approved by the Animal Care and Use Committee of Sichuan University. Four adult female beagle dogs (11 to 13 kg) were obtained from the Laboratory Animal Center of Sichuan University (Chengdu, Sichuan). The animals were anesthetized by intramuscular injection of propofol (4 mg/kg). Under sterile conditions, a longitudinal skin incision about 10 mm in length was made by scalpel on the line of spine and then the samples were inserted into the muscle, and five samples were implanted into each side of spine. Under the same conditions of anesthesia, the distal femur condyle of beagle was also exposed using a lateral approach. Using a dental drill with low rotational drill speed, a cylindrical hole (diameter of 5 mm and depth of 8 mm) was created perpendicular to the distal femur and randomly filled with samples. Four as-operated beagles were randomly divided into two groups including PEKK and PEKK-B samples. At 24 weeks postoperatively, all beagles were euthanized, and the implants with the surrounding tissues were harvested. Before the analysis, the harvested specimens were fixed in 4% paraformaldehyde solution for 7 days.

μ -CT evaluation

At 12 and 24 weeks postoperatively, a μ -CT imaging system was used to evaluate new bone formation within the implants of the harvested specimens ($n = 10$). During scanning, the cross sections of the specimens were imaged with a spot size of 7 μm and a maximum voltage of 70 kV. After being reconstructed with a high-resolution protocol, the obtained grayscale images were further analyzed using Scanco software, in which a global threshold was used to segment the newly formed bone tissue from each implant. After segmentation, the bone volume fraction was calculated by normalizing the bone volume to the total volume of the macropores of the implant.

Histological observation

After μ -CT evaluation, the specimens were dehydrated in ascending concentrations of alcohol from 75 to 100% and then embedded in polymethylmethacrylate. The embedded specimens were longitudinally cut into ~ 100 - μm -thick sections using a microtome (SAT-001, AoLiJing, China), followed by grinding and polishing to a final thickness of ~ 25 μm . The obtained sections were stained with methylene blue and basic fuchsin and toluidine blue for histological observation by a light microscope (Bx60, Olympus, USA) equipped with a digital charge-coupled device camera. The acquired microscope images were histologically evaluated using Image-Pro Plus software (Media Cybernetics, USA) for quantitative analysis of newly formed bone tissue. During the process, the "segmentation" tool was used to quantitatively measure the area of new bone in the macropores of the implant. Moreover, the nonstained sections were coated with a thin layer of Au and then analyzed using FE-SEM equipped with an energy-dispersive x-ray.

In vitro cell culture

The purified BMSCs from BALB/C mouse were purchased from Cyagen Biosciences Inc. (Mucmx-01001, Suzhou, China) and cultured

in α -minimum essential medium (Hyclone, USA) containing 10% fetal bovine serum (Gibco, USA) and 1% antibiotics (penicillin/streptomycin) under 5% CO_2 atmosphere at 37°C. As shown in fig. S7, the purchased BMSCs showed clear outline and uniform morphology, which were mostly flat and polygonal. After sterilizing with 75% alcohol for 1.5 hours and rinsing with sterile phosphate-buffered saline (PBS) for three times, the specimens were placed in 24-well plates before 2-ml medium was introduced into each well to balance the culturing environment for 12 hours.

Cell morphology and viability

BMSCs were seeded on each sample at a density of 1×10^5 per well in 24-well plates and then cultured for 1, 3, and 5 days. At each time point, the cells were stained with fluorescein diacetate (Sigma-Aldrich, USA) for live cells (green) and propidium iodide (Sigma-Aldrich, USA) for dead cells (red) after being washed twice with PBS. The morphology of cells on different groups of materials was observed using SEM. Before observing, the samples were fixed in 2.5% glutaraldehyde for 12 hours and rinsed with PBS three times and then dehydrated in ascending concentrations of alcohols from 30 to 100%. For further observing morphology and quantifying cell spreading area, cells were stained with phalloidin-tetramethyl rhodamine isothiocyanate (Sigma-Aldrich, USA) and 4',6-diamidino-2-phenylindole dihydrochloride (Sigma-Aldrich, USA) to visualize cytoskeleton and cell nucleus. The spreading area of a single cell was quantitatively evaluated by using Image-Pro Plus 6.0 software (Media Cybernetics, USA), in which six randomized nonoverlapping fields in each sample were selected.

Cell viability of BMSCs on the samples was quantified by a CCK-8 reagent kit. Briefly, the cell medium was discarded, and fresh medium containing 10% CCK-8 was added into each well. After incubation for 2 hours at 37°C, 200 μl of the above solution was transferred into a 96-well plate. The optical density (OD) was measured at a wavelength of 450 nm by a multifunctional, full-wavelength microplate reader (Varioskan Flash, Thermo Fisher Scientific, USA). For the above assays, all experiments were performed in triplicate.

Gene expression

After culture for 3 and 5 days, RNA was extracted using the RNeasy Mini Kit (QIAGEN, Germany) after being washed twice with PBS. Concentration and purity of the extracted RNA were assessed using a NanoDrop 2000 ultraviolet spectrophotometer (Thermo Fisher Scientific, USA). Then, the total RNA was reverse-transcribed into cDNA using an iScript cDNA synthesis kit (Bio-Rad, CA, USA). qRT-PCR was performed using the SsoFast EvaGreen Supermix (Bio-Rad) in a CFX96 real-time thermocycler (Bio-Rad). All experiments were done in triplicate to obtain the average data.

Extracellular matrix mineralization

Alizarin Red S staining was used to evaluate the degree of extracellular matrix mineralization on different PEKK scaffolds. After culturing for 3 and 14 days, the samples were fixed in 75% ethanol for 1 hour and stained with 1% Alizarin Red S solution (pH 4.2; Solarbio, China) for 10 min. After rinsing with ultrapure water, the staining results were observed by optical microscopy. To quantify the effect of staining, all samples were eluted in aqueous cetylpyridinium chloride solution, and the corresponding OD values were measured at 567 nm.

Gene expression profile microarray

BMSCs were seeded on each sample at a density of 1×10^5 per well in 24-well plates and then cultured for 3 days. Total RNA was extracted and using TRIzol reagent (Invitrogen, USA) according to the manufacturer's protocol. After measuring the quantity and quality, RNA integrity was assessed by standard denaturing agarose gel electrophoresis. The microarray assay was performed using the Agilent Mouse Gene Expression Microarray (Agilent Technology, USA) containing more than 39,000 mouse gene probes. Briefly, total RNA from each sample was linearly amplified and labeled with Cy3-UTP (cyanine 3-labeled UTPs). After purifying, 1 μ g of each labeled RNA was fragmented by adding 11 μ l of blocking agent and 2.2 μ l of fragmentation buffer. After heating at 60°C for 30 min, the labeled RNA was diluted by adding hybridization buffer. One hundred microliters of hybridization solution was dispensed into the gasket slide and assembled to the gene expression microarray slide. The slides were incubated for 17 hours at 65°C in an Agilent hybridization oven. After washing and fixing, the hybridized arrays were scanned using an Agilent DNA microarray scanner (Agilent Technology, USA).

Agilent Feature Extraction software (version 11.0.1.1) was used to analyze acquired array images. Quantile normalization and subsequent data processing were performed using a GeneSpring GX v12.1 software package (Agilent Technology, USA). A *P* value of ≤ 0.05 and a fold change value of ≥ 1.5 were used to select the differentially expressed genes. Hierarchical clustering was performed using the R software. GO analysis was performed using topGO package in R environment for statistical computing and graphics, and pathway analysis was calculated by Fisher's exact test.

Pharmacological inhibition study

To investigate the role of ADCY9/cAMP/PKA signaling pathways in material-induced osteogenesis, the pharmacological inhibition study was performed on BMSCs cultured with the PEKK-B scaffolds. After seeding in PEKK-B scaffold, the conditioned medium containing PAK inhibitor H89 (10 μ M; Sigma-Aldrich, USA) or ADCY inhibitor SQ22536 (10 μ M; Sigma-Aldrich, USA) was added. The conditioned medium with inhibitor was refreshed every 2 days. BMSCs cultured in the samples were harvested at 3 days for Western blot analysis according to the following procedures. The total protein in cells was isolated, and the protein concentration was measured using a BCA (bicinchoninic acid) protein kit (Pierce, IL, USA). Equal aliquots of protein (15 mg) were heated in boiled water for 10 min in sample buffer and fractionated by 10% SDS-polyacrylamide gel (Invitrogen, CA, USA). Then, the obtained samples were further transferred onto nitrocellulose membranes and blocked for 1 hour in 1 \times tris-buffered saline with Tween 20 with 1% bovine serum albumin. After washing for three times, the membranes were incubated with primary antibodies against PKA, MEK, p-MEK, ERK, p-ERK, CREB, p-CREB, ALP, and β -actin (Cell Signaling Technology, MA, USA) overnight and then incubated with a horseradish peroxidase-conjugated secondary antibody (Santa Cruz Biotechnology, CA, USA) at 37°C for 1 hour. A ChemiDoc XRS+ image system with Image Lab software (Bio-Rad, USA) was used to visualize the protein bands, and the protein expression was normalized against the level of β -actin for each group. In addition, the cAMP concentration in BMSCs was evaluated quantitatively using a commercially available enzyme-linked immunosorbent assay kit (CUSABIO, China) according to the manufacturer's specifications.

In addition, the tissue engineering protocol (49) was performed to evaluate the effect of PEKK-B-mediated cAMP/PKA activation on ectopic bone formation. BMSCs were seeded in the PEKK scaffolds at a density of 2×10^5 cells per sample. After 3 days of in vitro culture, the PEKK scaffold loaded with BMSCs was implanted into the bilateral muscle pouches of male BALB/C mouse (~20 g). The implanted scaffolds were retrieved for histological analysis at 90 days postoperatively according to our previous study (28). Briefly, the samples were decalcified for 4 weeks and then cut into 5- μ m-thick sections. After blocking with 5% hydrogen peroxidase, the sections were incubated with primary antibodies against OCN (Cell Signaling Technology, MA, USA), followed by washing and incubating with secondary antibodies. Then, the sections were incubated with avidin-biotin enzyme reagents and counterstained with hematoxylin.

Statistical analysis

All data were collected from at least three parallel samples for each test and expressed as means \pm SD, unless otherwise stated in the caption. Statistical analysis was carried out using the GraphPad Prism software (v6.0a; La Jolla, CA). Unpaired Student's *t* test was used for the comparisons between two groups, and one-way analysis of variance (ANOVA) with Tukey's post hoc test was used for the comparisons of three groups. Significant correlations were identified for *P* < 0.05. **P* < 0.05, ***P* < 0.01, and ****P* < 0.001.

SUPPLEMENTARY MATERIALS

Supplementary material for this article is available at <https://science.org/doi/10.1126/sciadv.abq7116>

[View/request a protocol for this paper from Bio-protocol.](#)

REFERENCES AND NOTES

1. S. Lin, G. Yang, F. Jiang, M. Zhou, S. Yin, Y. Tang, T. Tang, Z. Zhang, W. Zhang, X. Jiang, A magnesium-enriched 3D culture system that mimics the bone development microenvironment for vascularized bone regeneration. *Adv. Sci.* **6**, 1900209 (2019).
2. J. J. Li, C. R. Dunstan, A. Entezari, Q. Li, R. Steck, S. Saifzadeh, A. Sadeghpour, J. R. Field, A. Akey, M. Vielreicher, O. Friedrich, S. I. Roohani-Esfahani, H. Zreiqat, A novel bone substitute with high bioactivity, strength, and porosity for repairing large and load-bearing bone defects. *Adv. Healthc. Mater.* **8**, e1801298 (2019).
3. T. Maruyama, R. Stevens, A. Boka, L. DiRienzo, C. Chang, H. I. Yu, K. Nishimori, C. Morrison, W. Hsu, BMP1A maintains skeletal stem cell properties in craniofacial development and craniosynostosis. *Sci. Transl. Med.* **13**, eabb4416 (2021).
4. M. M. Stevens, Biomaterials for bone tissue engineering. *Mater. Today* **11**, 18–25 (2008).
5. S. Bhumiratana, J. C. Bernhard, D. M. Alfi, K. Yeager, R. E. Eton, J. Bova, F. Shah, J. M. Gimble, M. J. Lopez, S. B. Eising, G. Vunjak-Novakovic, Tissue-engineered autologous grafts for facial bone reconstruction. *Sci. Transl. Med.* **8**, 343ra83 (2016).
6. M. H. Hettiaratchi, L. Krishnan, T. Rouse, C. Chou, T. C. McDevitt, R. E. Guldberg, Heparin-mediated delivery of bone morphogenetic protein-2 improves spatial localization of bone regeneration. *Sci. Adv.* **6**, eaay1240 (2020).
7. G. L. Koons, M. Diba, A. G. Mikos, Materials design for bone-tissue engineering. *Nat. Rev. Mater.* **5**, 584–603 (2020).
8. S. J. Wang, D. Jiang, Z. Z. Zhang, Y. R. Chen, Z. D. Yang, J. Y. Zhang, J. Shi, X. Wang, J. K. Yu, Biomimetic nanosilica-collagen scaffolds for in situ bone regeneration: Toward a cell-free, one-step surgery. *Adv. Mater.* **31**, e1904341 (2019).
9. S.-S. Jin, D.-Q. He, D. Luo, Y. Wang, M. Yu, B. Guan, Y. Fu, Z.-X. Li, T. Zhang, Y.-H. Zhou, C.-Y. Wang, Y. Liu, A biomimetic hierarchical nanointerface orchestrates macrophage polarization and mesenchymal stem cell recruitment to promote endogenous bone regeneration. *ACS Nano* **13**, 6581–6595 (2019).
10. H. Xia, X. Li, W. Gao, X. Fu, R. H. Fang, L. Zhang, K. Zhang, Tissue repair and regeneration with endogenous stem cells. *Nat. Rev. Mater.* **3**, 174–193 (2018).
11. Z. Xingdong, D. Williams, *Definitions of Biomaterials for the Twenty-First Century* (Elsevier, 2019).
12. G. D. Winter, B. J. Simpson, Heterotopic bone formed in a synthetic sponge in the skin of young pigs. *Nature* **223**, 88–90 (1969).
13. L. L. Hench, J. M. Polak, Third-generation biomedical materials. *Science* **295**, 1014–1017 (2002).

14. J. C. Doloff, O. Veisoh, R. de Mezerville, M. Sforza, T. A. Perry, J. Haupt, M. Jamiel, C. Chambers, A. Nash, S. Aghlari-Fotovat, J. L. Stelzel, S. J. Bauer, S. Y. Neshat, J. Hancock, N. A. Romero, Y. E. Hidalgo, I. M. Leiva, A. M. Munhoz, A. Bayat, B. M. Kinney, H. C. Hodges, R. N. Miranda, M. W. Clemens, R. Langer, The surface topography of silicone breast implants mediates the foreign body response in mice, rabbits and humans. *Nat. Biomed. Eng.* **5**, 1115–1130 (2021).
15. R. Xie, H. Yao, A. S. Mao, Y. Zhu, D. Qi, Y. Jia, M. Gao, Y. Chen, L. Wang, D. A. Wang, K. Wang, S. Liu, L. Ren, C. Mao, Biomimetic cartilage-lubricating polymers regenerate cartilage in rats with early osteoarthritis. *Nat. Biomed. Eng.* **5**, 1189–1201 (2021).
16. N. Huebsch, D. J. Mooney, Inspiration and application in the evolution of biomaterials. *Nature* **462**, 426–432 (2009).
17. Z. Xingdong, Z. Pin, Z. Jianguo, C. Weiqun, W. Chuang, A study of porous block HA ceramics and its osteogenesis, in *Bioceramics and the Human Body* (Elsevier, 1991), pp. 408–415.
18. U. Ripamonti, Bone induction in nonhuman primates an experimental study on the baboon. *Clin. Orthop. Relat. Res.* 284–294 (1991).
19. Z. Yang, H. Yuan, W. Tong, P. Zou, W. Chen, X. Zhang, Osteogenesis in extraskeletally implanted porous calcium phosphate ceramics variability among different kinds of animals. *Biomaterials* **17**, 2131–2137 (1996).
20. H. Yuan, H. Fernandes, P. Habibovic, J. de Boer, A. M. Barradas, A. de Ruyter, W. R. Walsh, C. A. van Blitterswijk, J. D. de Bruijn, Osteoinductive ceramics as a synthetic alternative to autologous bone grafting. *Proc. Natl. Acad. Sci. U.S.A.* **107**, 13614–13619 (2010).
21. R. M. Parker, G. M. Malham, Comparison of a calcium phosphate bone substitute with recombinant human bone morphogenetic protein-2: A prospective study of fusion rates, clinical outcomes and complications with 24-month follow-up. *Eur. Spine J.* **26**, 754–763 (2017).
22. S. Fujibayashi, M. Neo, H.-M. Kim, T. Kokubo, T. Nakamura, Osteoinduction of porous bioactive titanium metal. *Biomaterials* **25**, 443–450 (2004).
23. U. Ripamonti, L. C. Roden, L. F. Renton, Osteoinductive hydroxyapatite-coated titanium implants. *Biomaterials* **33**, 3813–3823 (2012).
24. M. Lu, H. Chen, B. Yuan, Y. Zhou, L. Min, Z. Xiao, X. Yang, X. Zhu, C. Tu, X. Zhang, The morphological effect of nanostructured hydroxyapatite coatings on the osteoinduction and osteogenic capacity of porous titanium. *Nanoscale* **12**, 24085–24099 (2020).
25. S. M. Kurtz, J. N. Devine, PEEK biomaterials in trauma, orthopedic, and spinal implants. *Biomaterials* **28**, 4845–4869 (2007).
26. R. F. Kersten, S. M. van Gaalen, A. de Gast, F. C. Oner, Polyetheretherketone (PEEK) cages in cervical applications: A systematic review. *Spine J.* **15**, 1446–1460 (2015).
27. B. Yuan, Q. Cheng, R. Zhao, X. Zhu, X. Yang, X. Yang, K. Zhang, Y. Song, X. Zhang, Comparison of osteointegration property between PEKK and PEEK: Effects of surface structure and chemistry. *Biomaterials* **170**, 116–126 (2018).
28. B. Yuan, L. Wang, R. Zhao, X. Yang, X. Yang, X. Zhu, L. Liu, K. Zhang, Y. Song, X. Zhang, A biomimetically hierarchical polyetheretherketone scaffold for osteoporotic bone repair. *Sci. Adv.* **6**, eabc4704 (2020).
29. J. W. Williams, K. Zaitsev, K. W. Kim, S. Ivanov, B. T. Saunders, P. R. Schrank, K. Kim, A. Elvington, S. H. Kim, C. G. Tucker, M. Wohltmann, B. T. Fife, S. Epelman, M. N. Artyomov, K. J. Lavine, B. H. Zinselmeyer, J. H. Choi, G. J. Randolph, Limited proliferation capacity of aortic intima resident macrophages requires monocyte recruitment for atherosclerotic plaque progression. *Nat. Immunol.* **21**, 1194–1204 (2020).
30. G. Campanella, M. G. Hanna, L. Geneslaw, A. Mirafior, V. W. K. Silva, K. J. Busam, E. Brogi, V. E. Reuter, D. S. Klimstra, T. J. Fuchs, Clinical-grade computational pathology using weakly supervised deep learning on whole slide images. *Nat. Med.* **25**, 1301–1309 (2019).
31. X. Chen, X. Kong, W. Zhuang, B. Teng, X. Yu, S. Hua, S. Wang, F. Liang, D. Ma, S. Zhang, X. Zou, Y. Dai, W. Yang, Y. Zhang, Dynamic changes in protein interaction between AKAP95 and Cx43 during cell cycle progression of A549 cells. *Sci. Rep.* **6**, 1–13 (2016).
32. T. Zhao, M. Hou, M. Xia, Q. Wang, H. Zhu, Y. Xiao, Z. Tang, J. Ma, W. Ling, Globular adiponectin decreases leptin-induced tumor necrosis factor- α expression by murine macrophages: Involvement of cAMP-PKA and MAPK pathways. *Cell. Immunol.* **238**, 19–30 (2005).
33. O. Omar, T. Engstrand, L. K. B. Linder, J. Aberg, F. A. Shah, A. Palmquist, U. Birgersson, I. Elgali, M. Pujari-Palmer, H. Engqvist, P. Thomsen, In situ bone regeneration of large cranial defects using synthetic ceramic implants with a tailored composition and design. *Proc. Natl. Acad. Sci. U.S.A.* **117**, 26660–26671 (2020).
34. M. Zhang, R. Lin, X. Wang, J. Xue, C. Deng, C. Feng, H. Zhuang, J. Ma, C. Qin, L. Wan, J. Chang, C. Wu, 3D printing of Haversian bone-mimicking scaffolds for multicellular delivery in bone regeneration. *Sci. Adv.* **6**, eaaz6725 (2020).
35. S. Chen, H. Wang, V. L. Mainardi, G. Talò, A. McCarthy, J. V. John, M. J. Teusink, L. Hong, J. Xie, Biomaterials with structural hierarchy and controlled 3D nanotopography guide endogenous bone regeneration. *Sci. Adv.* **7**, eabg3089 (2021).
36. Z. Tang, X. Li, Y. Tan, H. Fan, X. Zhang, The material and biological characteristics of osteoinductive calcium phosphate ceramics. *Regen. Biomater.* **5**, 43–59 (2018).
37. M. Bohner, R. J. Miron, A proposed mechanism for material-induced heterotopic ossification. *Mater. Today* **22**, 132–141 (2019).
38. B. Yuan, Y. Chen, H. Lin, Y. Song, X. Yang, H. Tang, E. Xie, T. Hsu, X. Yang, X. Zhu, K. Zhang, X. Zhang, Processing and properties of bioactive surface-porous PEKK. *ACS Biomater. Sci. Eng.* **2**, 977–986 (2016).
39. N. T. Evans, F. B. Torstrick, C. S. Lee, K. M. Dupont, D. L. Safranski, W. A. Chang, A. E. Macedo, A. S. Lin, J. M. Boothby, D. C. Whittingslow, R. A. Carson, R. E. Goldberg, K. Gall, High-strength, surface-porous polyether-ether-ketone for load-bearing orthopedic implants. *Acta Biomater.* **13**, 159–167 (2015).
40. Z. Othman, H. Fernandes, A. J. Groot, T. M. Luider, A. Alcinesio, D. M. Pereira, A. P. M. Guttenplan, H. Yuan, P. Habibovic, The role of ENPP1/PC-1 in osteoinduction by calcium phosphate ceramics. *Biomaterials* **210**, 12–24 (2019).
41. R. M. Klar, R. Duarte, T. Dix-Peek, C. Dickens, C. Ferretti, U. Ripamonti, Calcium ions and osteoclastogenesis initiate the induction of bone formation by coral-derived macroporous constructs. *J. Cell. Mol. Med.* **17**, 1444–1457 (2013).
42. Z. Tang, S. Chen, Y. Ni, R. Zhao, X. Zhu, X. Yang, X. Zhang, Role of Na⁺, K⁺-ATPase ion pump in osteoinduction. *Acta Biomater.* **129**, 293–308 (2021).
43. N. Groen, H. Yuan, D. G. Hebls, G. Kocer, F. Mbuyi, V. LaPointe, R. Truckenmuller, C. A. van Blitterswijk, P. Habibovic, J. de Boer, Linking the transcriptional landscape of bone induction to biomaterial design parameters. *Adv. Mater.* **29**, 1603259 (2017).
44. R. Siddappa, A. Martens, J. Doorn, A. Leusink, C. Olivo, R. Licht, L. van Rijn, C. Gaspar, R. Fodde, F. Janssen, C. van Blitterswijk, J. D. Boer, cAMP-PKA pathway activation in human mesenchymal stem cells in vitro results in robust bone formation in vivo. *Proc. Natl. Acad. Sci. U.S.A.* **105**, 7281–7286 (2008).
45. C. W. Dessauer, V. J. Watts, R. S. Ostrom, M. Conti, S. Dove, R. Seifert, International union of basic and clinical pharmacology. CI. Structures and small molecule modulators of mammalian adenylyl cyclases. *Pharmacol. Rev.* **69**, 93–139 (2017).
46. K. L. Lee, D. A. Hoey, M. Spasic, T. Tang, H. K. Hammond, C. R. Jacobs, Adenylyl cyclase 6 mediates loading-induced bone adaptation in vivo. *FASEB J.* **28**, 1157–1165 (2014).
47. M. G. Cumbay, V. J. Watts, Galphag potentiation of adenylyl cyclase type 9 activity through a Ca²⁺/calmodulin-dependent pathway. *Biochem. Pharmacol.* **69**, 1247–1256 (2005).
48. Y. R. Shih, Y. Hwang, A. Phadke, H. Kang, N. S. Hwang, E. J. Caro, S. Nguyen, M. Siu, E. A. Theodorakis, N. C. Gianneschi, K. S. Vecchio, S. Chien, O. K. Lee, S. Varghese, Calcium phosphate-bearing matrices induce osteogenic differentiation of stem cells through adenosine signaling. *Proc. Natl. Acad. Sci. U.S.A.* **111**, 990–995 (2014).
49. C. Trojani, F. Boukhechba, J. C. Scimeca, F. Vandenbos, J. F. Michiels, G. Daculsi, P. Boileau, P. Weiss, G. F. Carle, N. Rochet, Ectopic bone formation using an injectable biphasic calcium phosphate/Si-HPMC hydrogel composite loaded with undifferentiated bone marrow stromal cells. *Biomaterials* **27**, 3256–3264 (2006).

Acknowledgments

Funding: This project was funded by the National Key Research and Development Program of China (2016YFC1102000 and 2020YFB1711500), the National Natural Science Foundation of China (32101080), the China Postdoctoral Science Foundation (2021M692316 and 2020TQ0218), and the Fundamental Research Funds for the Central Universities (2021SCU12071). **Author contributions:** B.Y., X.D.Z., and K.Z. were responsible for the experimental concept and design. B.Y., Y.Z., and R.Z. prepared the materials, performed the studies, and analyzed the data. R.Z., X.Y., and H.L. performed μ -CT evaluation and analyzed the data. B.Y. and X. Zhu wrote the manuscript, and K.Z., A.G.M., and X. Zhang edited the manuscript. All authors reviewed and approved the manuscript before publication. **Competing interests:** The authors declare that they have no competing interests. **Data and materials availability:** All data needed to evaluate the conclusions in the paper are present in the paper and/or the Supplementary Materials.

Submitted 26 April 2022

Accepted 17 August 2022

Published 5 October 2022

10.1126/sciadv.abq7116